SUPPLEMENTARY INFORMATION

Tuning the Optical and Electronic Properties of Colloidal Nanocrystals by Lattice Strain

Andrew M. Smith, Aaron M. Mohs, and Shuming Nie

Departments of Biomedical Engineering and Chemistry, Emory University and Georgia Institute of Technology, 101 Woodruff Circle, Suite 2001, Atlanta, Georgia 30322, USA

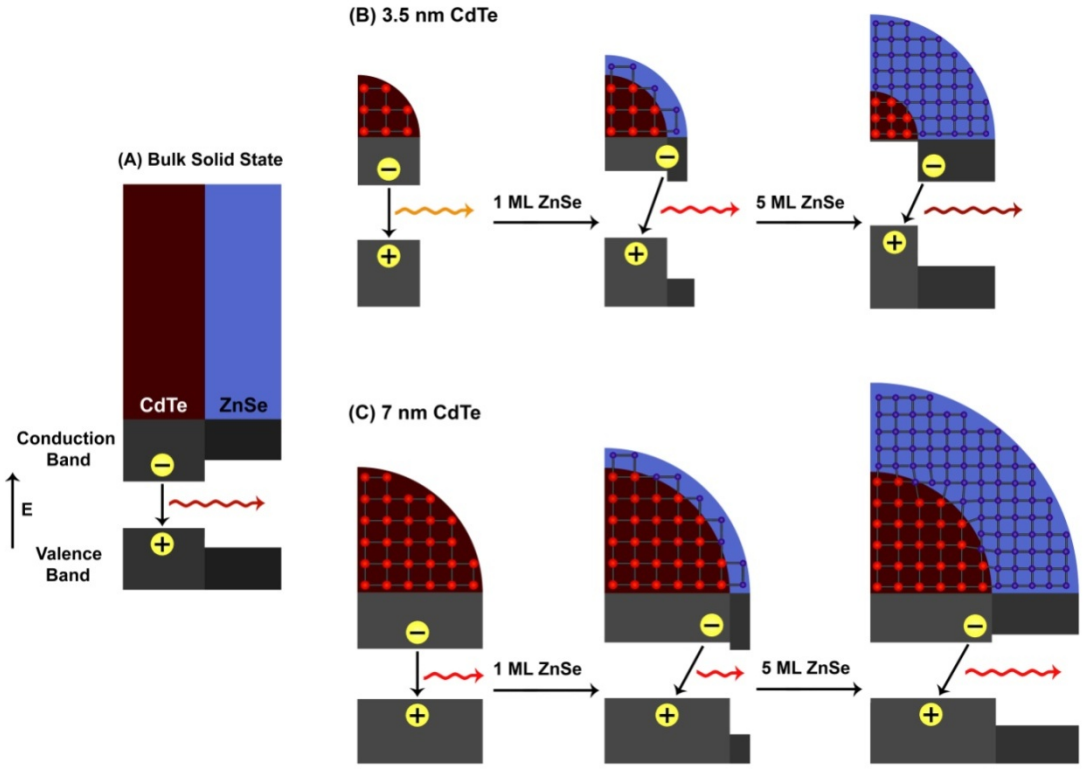

Supplementary Figure 1. Diagrams illustrating the effects of strain tuning for small (3.8 nm) and large (7.0 nm) CdTe nanocrystals, and the concept of "quasi type-II" structures. (A) As a bulk heterostructure, the interface between CdTe and ZnSe yields a type-I band alignment, with the conduction band energy minimum and valence band energy maximum located in the CdTe domain. The bulk bandgap is 1.50 eV for CdTe and 2.82 eV for ZnSe. **(B)** The charge carriers in a small CdTe QDs (3.5 nm) are quantum-confined, thus increasing the bandgap energy (~2.0 eV). As well, the electronic energy levels become discrete (not depicted). With overgrowth of a thin shell of ZnSe (1 monolayer, ML), the core is slightly compressed due to the smaller lattice parameter of ZnSe (5.668 Å) compared to CdTe (6.482

Å), increasing the energy of the CdTe conduction band. The shell material is under large tensile strain due to coherent growth on the CdTe substrate, resulting in a significant reduction of the conduction band in the shell. Because of these simultaneous shifts, there is only a very small difference in energy between the conduction bands of the core and shell, causing the electron wavefunction to spread across the entire nanocrystal. Quantum confinement and strain have a smaller impact on the valence bands, and the hole remains in the core, leading to a quasi type-II structure, in which the hole is strongly confined, but the electron is delocalized over the entire QD. Overgrowth of a larger shell (5 ML) further increases the core conduction band energy and decreases the conduction band energy in the shell. Thus the band offsets become staggered, shifting the electron almost entirely into the shell material, resulting in a type-II material that has a smaller indirect bandgap, and therefore a longer wavelength of emission. **(C)** Using a larger CdTe core (7 nm), the quantum confinement effect is reduced, decreasing the bandgap (~1.7 eV). Overgrowth of a thin shell of ZnSe (1 ML) strongly strains the shell, with little effect on the core material due to the large core size compared to the volume of the shell. The electron is likely to be weakly delocalized over the entire nanocrystal, again yielding a quasi-type-II band structure. However, for this core size, growth of a larger shell (5 ML) exceeds the critical thickness, and can only be accommodated by the formation of defects that relax the strain between the two materials. Therefore the core and shell materials are under little strain, returning their band offsets to near that of their bulk values.

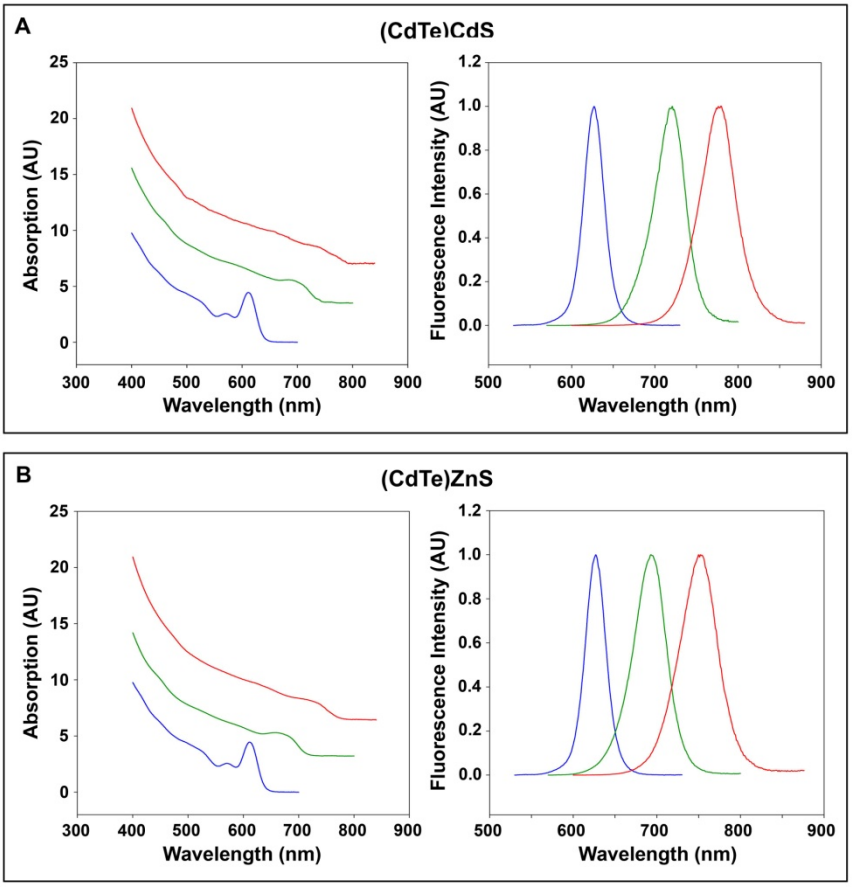

Supplementary Figure 2. **Optical absorption (left) and fluorescence emission (right) of strain-tunable CdTe QDs prepared by using CdSe or ZnS as the shell material.** The shell thicknesses are 0 (blue), 2 (green), or 4 (red) monolayers.

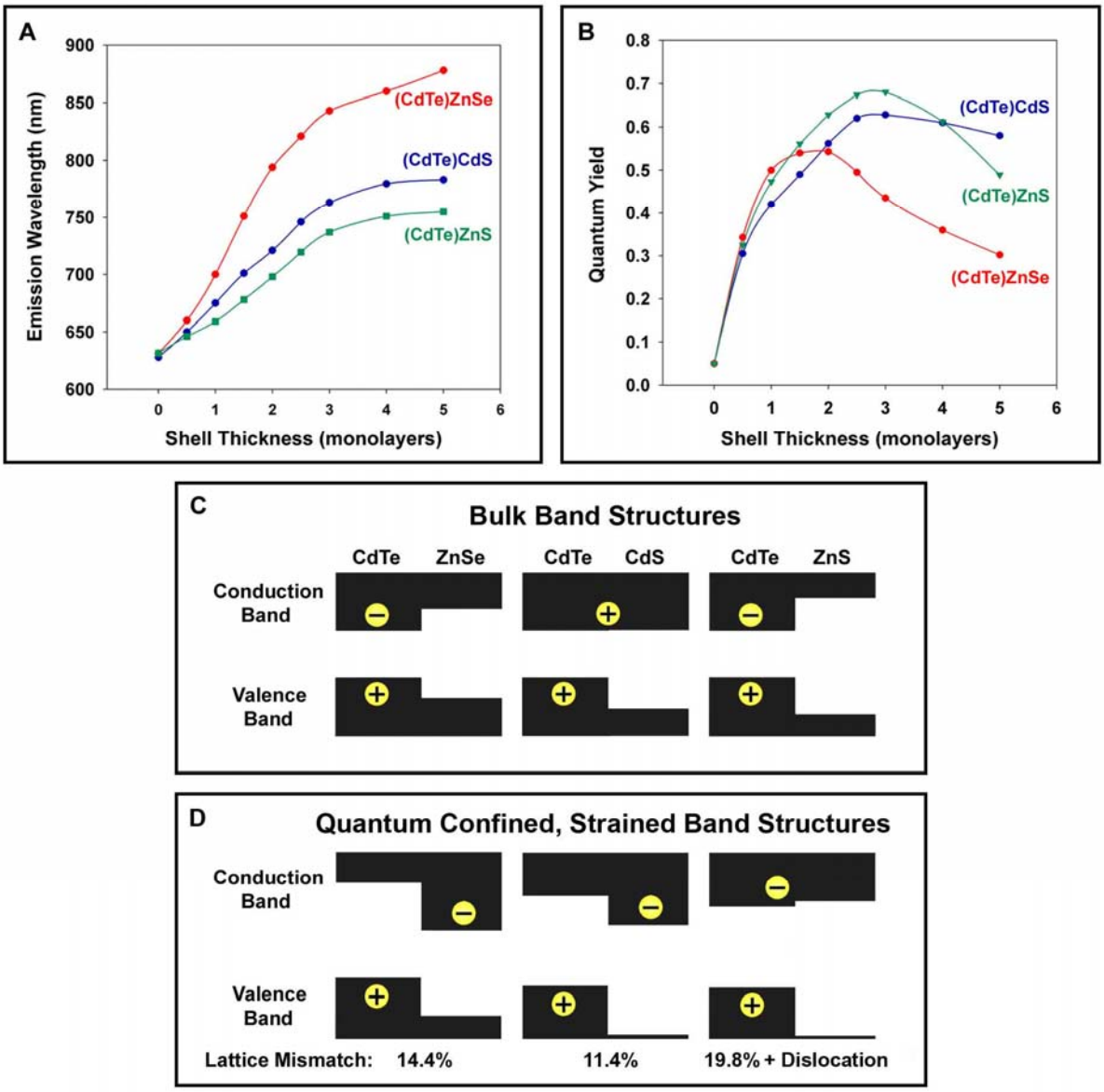

Supplementary Figure 3. Comparison of optical tunability and fluorescence quantum yields for CdTe cores coated with different shell materials and thicknesses. (**A**) Emission wavelengths of 3.8 nm CdTe cores capped with ZnSe, CdS, or ZnS as a function of shell thickness. (**B**) Fluorescence quantum yields of the same QDs plotted as a function of shell thickness. (**C**) Diagrams of bulk band offsets for core/shell structures in (**A**) and (**B**). (**D**) Diagrams of band offsets for core/shell nanocrystals, accounting for the impacts of quantum confinement and strain, calculated by using model-solid theory and a continuum elasticity model. In this model, we find that the (CdTe)ZnS core/shell QD is not coherent beyond ~3 monolayers of shell growth, and therefore a single dislocation loop and its associated strain relaxation are included in the band structure calculations.

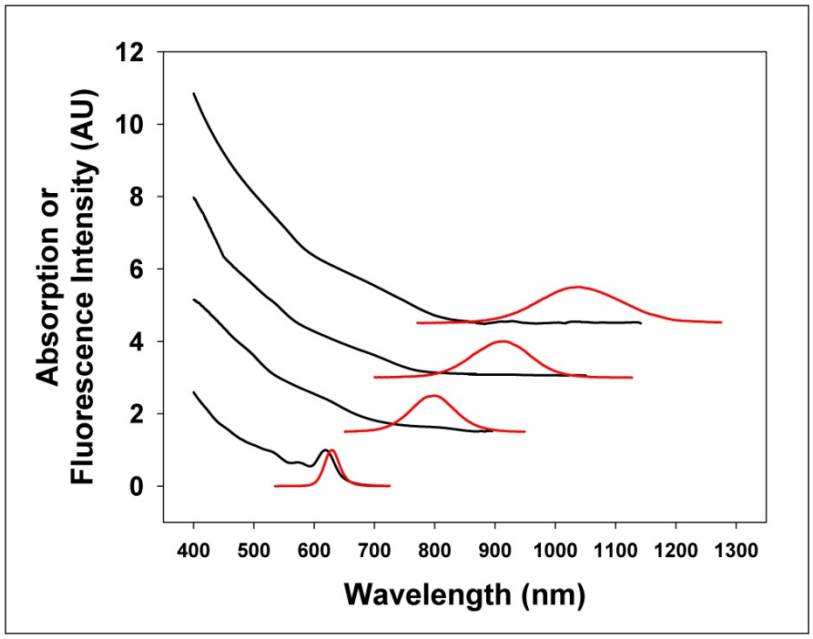

Supplementary Figure 4. Absorption (black) and fluorescence emission (red) spectra obtained from (CdTe)ZnSe QDs with shell thicknesses ranging from o to 9 monolayers. depicted in TEMs in Figure 4 of the main body of the text. From bottom to top, the 3.8 nm CdTe cores are capped with 0, 2, 6, or 9 monolayers of ZnSe.

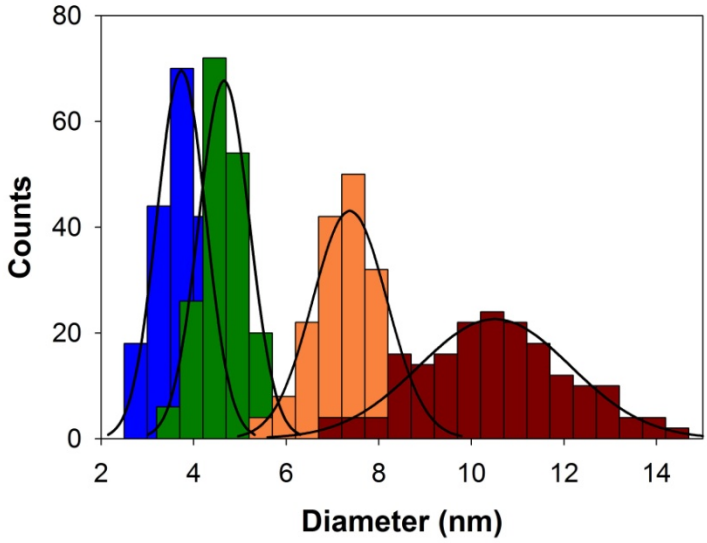

Supplementary Figure 5. **Particle size distributions obtained directly from TEM images of (CdTe)ZnSe QDs.** Average sizes are 3.75 ± 0.53 nm for CdTe cores (blue), 4.66 ± 0.55 nm for 2 ML shell (green), 7.37 ± 0.81 nm for 6 ML shell (orange), and 10.51 ± 1.64 nm for 9 ML shell (red). For each sample, ~180 particles are measured, and are reported as mean diameter ± standard deviation.

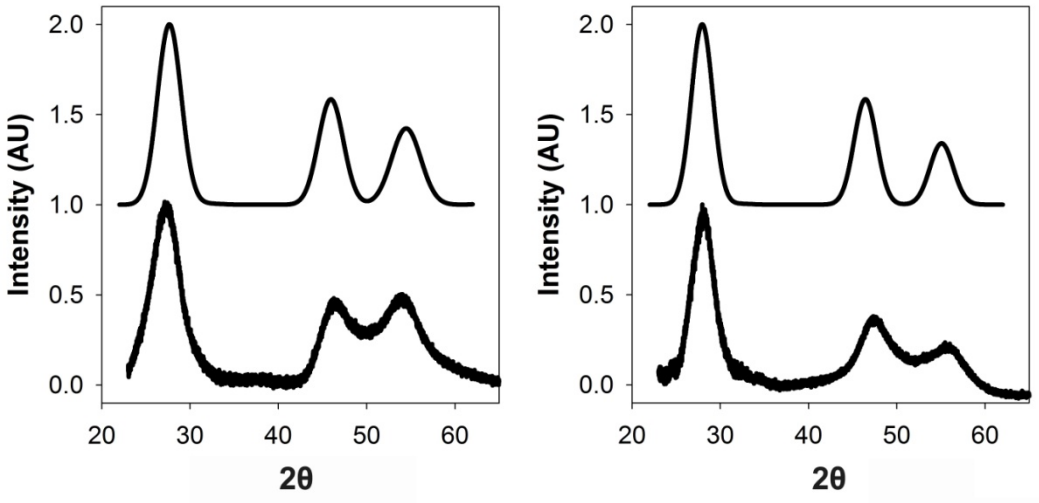

Supplementary Figure 6. Comparison of simulated (upper) and experimental (lower) c-ray diffraction data for (CdTe)ZnSe QDs (Figure 4A). Left: CdTe cores modeled as hexagonal cylinders composed of ~850 atoms with a diameter of 3.2 nm and a length of 4.4 nm, elongated in the [111] zinc blende lattice direction. Right: Core/shell (CdTe)ZnSe nanocrystals modeled with a nonrelaxed, radially concentric shell of ZnSe (two monolayers or approximately 2000 atoms). Stacking faults, which have been shown to be common in the [001] direction for wurtzite CdSe, are included in our simulations because of the dearth of knowledge of their abundance in small zinc blende CdTe nanocrystals.

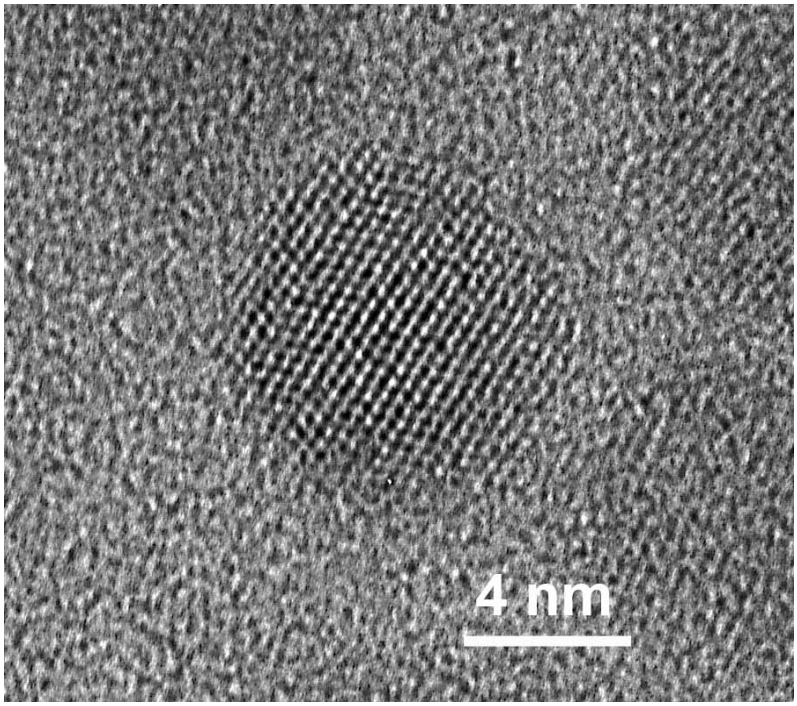

Supplementary Figure 7. Enlarged high-resolution TEM micrograph showing a 3.8 nm CdTe QD coated with 6 monolayers of ZnSe with multiple twinning.

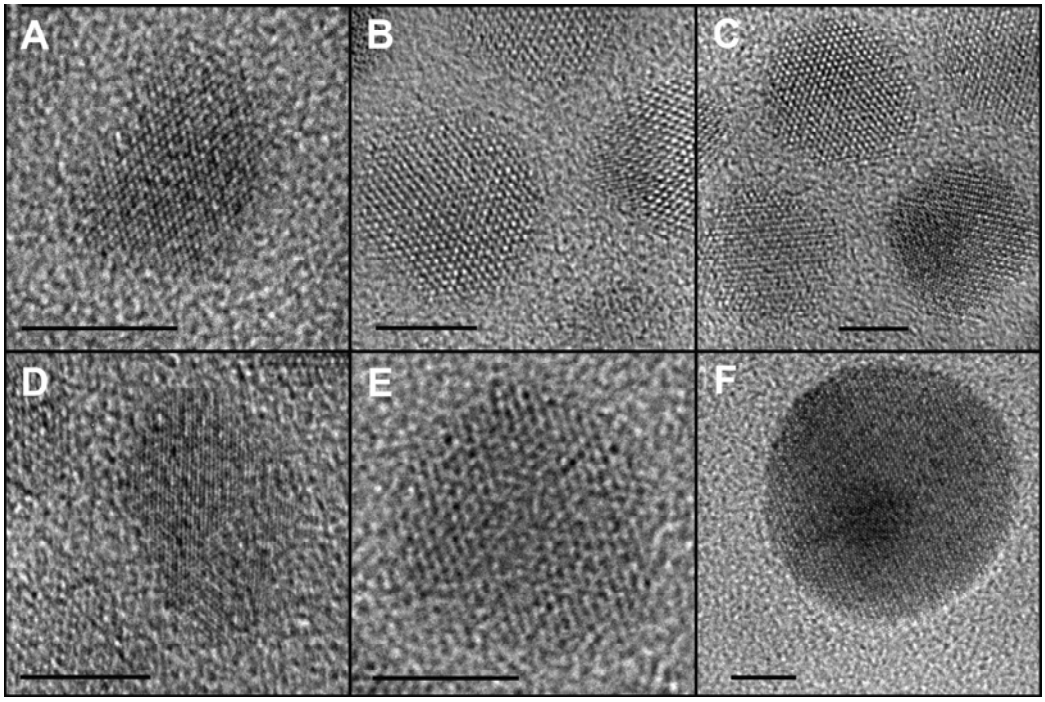

Supplementary Figure 8. High-resolution TEM images of (core)shell (CdTe)ZnSe quantum dots demonstrating lattice warping and localized differences in electron density at different shell thicknesses. Shell thicknesses are 3 monolayers (A), 6 monolayers (B-E), or ~10 monolayers (F). Scale bars represent 5 nm.

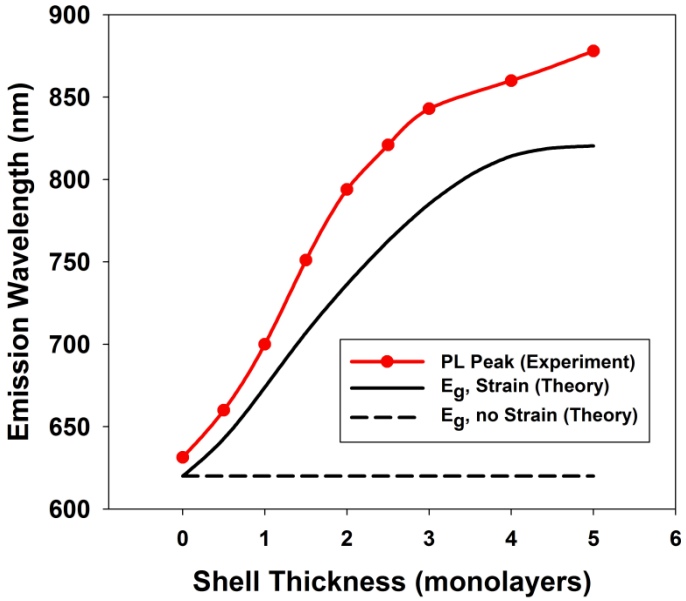

Supplementary Figure 9. Comparison of experimentally measured photoluminescence (PL) emission wavelengths with predicted bandgap values calculated by using a continuum elasticity model and the model-solid theory. The experimental data points are obtained from 3.8 nm CdTe QDs coated with 0 to 5 monolayers of ZnSe shell (reproduced from Figure 3A). The theoretical data are implemented from concentric cylinders, with (black solid line) or without strain (black

hatched line). When accounting for quantum confinement of the materials, the QD was determined to be type I when the effects due to strain are ignored. With strain, the bandgap decreases due to the formation of a type-II structure. The disparity between the experimental PL peak and the predicted energy gap is due to a combination of the Stokes shift between the absorption band edge and the PL peak, and shortcomings of the model.

Supplementary Table 1. Summary of Line-Width Analysis Data for (CdTe)ZnSe QDs with Different Shell Thicknesses.

Composition	Lattice constant	Lattice plane	Domain size (nm)
CdTe	FCC, a = 6.49 Å	(111)	3.44
		(220)	4.01
(CdTe)ZnSe, 2 ML	FCC, a = 6.41 Å	(111)	4.20
(CdTe)ZnSe, 6 ML	HCP, a = 4.36 Å	(220)	8.02
	c = 7.12 Å	(112)	6.58
(CdTe)ZnSe, 9 ML	HCP, a = 4.35 Å	(100)	14.38
	c = 7.10 Å	(002)	10.41
		(101)	9.06
		(110)	15.87
		(112)	12.05

Some peaks, such as the (311) reflection for the core QDs, are associated with substantial background scattering, and are not evaluated. The lattice constants are calculated by averaging the reflections.

Supplementary Table 2. List of Experimental Parameters for Synthesis of Strain-Tunable (CdT)ZnSe QDs.

CdTe core size	[QD]	T_{OW}	T_{ML1}	T_{ML2}	T_{ML3-4}	T_{ML5-6}	T_{ML7-9}
1.8 nm	28 μM	150ºC	140ºC	190ºC	225ºC	250ºC	n.a.
3.8 nm	6.0 μM	170ºC	150ºC	225ºC	225ºC	250ºC	260ºC
5.2 nm	4.0 μM	210ºC	190ºC	225ºC	225ºC	250ºC	n.a.
6.2 nm	3.0 μM	230ºC	225ºC	225ºC	225ºC	250ºC	n.a.

[QD] is the QD concentration used for shell growth; T_{OW} is the temperature of onset of Ostwald ripening; and $T_{ML\#}$ is the growth temperature for various shell monolayers. Growth of shells thicker than 6 ML is only performed on 3.8-nm CdTe cores.

Supplementary Table 3. Summary of Shell Thickness Data

Shell thickness	n_{ZnSe} / n_{QD}	d_{obs} (nm)	$d_{T\text{-}S}$ (nm) relaxed	$d_{T\text{-}S}$ (nm) strained	$d_{T\text{-}C}$ (nm) relaxed	$d_{T\text{-}C}$ (nm) strained
0 (core)	n.a.	3.75	n.a.	n.a.	n.a.	n.a.
2 ML	595	4.66	4.74	5.04	4.22	4.60
6 ML	3071	7.37	6.85	7.31	7.08	7.79
9 ML	6446	10.51	8.50	9.20	9.71	10.91

Shell growth of ZnSe on ~3.8 nm CdTe cores is performed as described in **Methods**. The total amount of each precursor added is tabulate as the number of moles of ZnSe per mole of QD (n_{ZnSe} / n_{QD}). The resulting nanocrystal diameter (d_{obs}) is determined via TEM. Four types of theoretically calculated diameters (d_T) are shown, assuming either spherical growth ($d_{T\text{-}S}$) or growth in the radial direction on a cylindrical core ($d_{T\text{-}C}$), with or without lattice strain. The observed sizes indicate that coherent shell growth proceeds in a manner that is intermediate between spherical and cylindrical.

Supplementary Discussion. From the perspective of quantum confinement of electronic energy states, as the dimensions of the heterostructure decrease from bulk to that of the core-shell QD, the corresponding widening of the bandgap may occur asymmetrically between the bands of the core and shell, thus altering the band offsets between the materials. If this is the case, when the ZnSe shell thickness increases, its conduction band edge would decrease in energy, below that of the conduction band of the highly confined CdTe core, thus increasing electron density in the shell, and yielding a type-II structure. This rationale has been proposed as a mechanism for modulating between type-I and type-II character in (ZnSe)CdSe and (CdS)ZnSe core/shell QDs by adjusting the shell thickness.[4,5] However we do not find this to be an adequate explanation for the (CdTe)ZnSe system because the bulk conduction band offsets (ΔE_c=0.68 eV) and valence band offsets (ΔE_v=0.64 eV) are similar, and despite large differences in electron and hole effective masses, the relative bandshifts should not be tremendously different. Moreover, if this were the case, CdS would be an even better shell material for generating type-II QDs with CdTe cores, due to the near-zero conduction band offset between these materials in bulk, and because the effective masses of its charge carriers are comparable to those of ZnSe.[6] (CdTe)CdS QDs indeed did demonstrate quasi-type-II character after thick shells were grown (≥ 5 monolayers), however the magnitude of spectral shifting was much less than that of (CdTe)ZnSe (**Suppl Figures 2 & 3**).

Alloying of the two materials at the CdTe/ZnSe interface could also generate a type-II structure. Diffusion of either zinc or selenium from the shell into the core could result in ZnTe/CdSe or CdTe/CdSe/ZnTe interfaces, respectively, which are both type-II heterostructures in bulk. Indeed, Cd(Te,Se) QDs grown via self-assembly on a ZnSe substrate using molecular beam epitaxy show two emission bands, one attributed to

Cd(Te,Se) type-I QD emission, and another to lower energy type-II behavior, believed to be due to a ZnSeTe/ZnSe interface.[7] However we find an alloying mechanism to be unsatisfactory, due to the fact that this band shift is highly dependent on the size of the QD core (**Figure 2C**), and type-II character is not evident for core-shell QDs with cores larger than ~5 nm diameter (**Figure 2B, 2C**). Also supporting this argument is that most other (core)shell QDs such as (CdSe)ZnS and (CdSe)CdS have not been observed to undergo significant interatomic rearrangements, even at elevated temperatures.[2,8] As well, this type-II nature does not develop until thicker shells are grown on the QDs (2-3 monolayers), whereas type-II QDs would be predicted to have formed with only thin shells within this model because (CdTe)CdSe has strong type-II characteristics after 1 monolayer of shell growth. Alternatively, it is possible that the strain within the CdTe (6.48 Å lattice constant) core caused by the compressive ZnSe (5.67 Å lattice constant) shell induces an indirect bandgap in the CdTe QD, as previously observed for small InP QDs that transition from direct to indirect semiconductors under hydrostatic pressure.[33,34] We find this to be unlikely because the band shifts of the photoluminescence and absorption spectra are gradual with shell growth, which would not reflect a pressure-induced direct-to-indirect semiconductor transition, in which the direct band-edge commonly disappears suddenly, leading to the appearance of an indirect edge and very low photoluminescence efficiencies.

To explain the QD phase change from zinc blende to wurtzite, it has been calculated that there is only a very small difference in energy between these two phases for most II-VI materials (<10 meV per atom).[9,10] In particular, the cubic zinc blende phase has been found to be the more stable bulk crystal structure for both ZnSe and CdTe, with only a small energy advantage over the wurtzite structure (E_{WZ-ZB} = 5.3 meV per atom for ZnSe, and E_{WZ-ZB} = 4.5 meV per atom for CdTe). This energy difference is only a small fraction (~0.2%) of the bond energy within the crystal itself (E_{ZnSe} = 1.29 eV per bond, E_{CdTe} = 1.1 eV per bond). Thus minute changes to the crystal and its environment can favor one of the phases over the other, and even induce a phase transition to the metastable wurtzite phase. This especially holds true for nanocrystals, in which the state of the surface atoms can account for a large fraction of the particle.[11,12] For nanocrystals, the growth temperature, the chemical nature of organic passivating ligands, and heteroepitaxial growth have all been found to modulate the crystalline phase for II-VI semiconductors (notably ZnSe, CdSe, and CdTe). Indeed, nanocrystals composed of ZnSe or CdTe have been prepared with a variety of shapes in both wurtzite and zinc blende structures, demonstrating that the energy separation between these two phases can be overcome on the nanoscale.[12-15] Two important facors in governing phase modulations are discussed in more details below:

(a) *Reaction conditions*. In the preparation of CdTe QD cores, our production of cubic CdTe QDs is expected from the use of strongly binding alkylphosponic acid ligands, which have been shown in previous studies to favor the zinc blende phase.[12,16] These ligands are removed from the reaction solution via extraction prior to shell growth, which is performed in the presence of weaker ligands (phosphines and amines), which may favor the growth of wurtzite crystals. Similar solvent systems have been used to generate wurtzite ZnSe nanocrystals,[13,14,17] and have also been used to

synthesize ZnSe/CdSe QDs in which the phases are similarly transformed from cubic to wurtzite during crystal growth.[18] The temperature of growth may also factor into this procedure, but its role is difficult to discern, as this process requires an increase in temperature to grow larger shells. Larger nanocrystals are resistant to growth at lower temperatures, likely due to lower surface energy, and perhaps stronger binding to their ligands.

(b) Lattice strain. The compressibility of the wurtzite phase is known to be greater than that of the zinc blende phase, and thus some of the lattice strain energy may be alleviated through a phase transition.[10,19] Indeed, theoretical calculations have shown that strained heteroepitaxial growth of CdTe can reduce the energy of phase transition between zinc blende to wurtzite to zero, which agrees with experimental observations.[10] The compressibilities of the II-VI materials are also highly anisotropic, being more compressible along the wurtzite [001] direction (the c-axis). Our experimental observations from XRD and HRTEM reveal that the growth of the shell is primarily along the c-axis. Because this growth pattern is expected to compress the c-axis direction of the core, an increase in the compressibility could be attained in both the core and shell materials with a phase transition to the wurtzite phase, which should reduce the energy of elastic deformation.

Since the nanocrystals are primarily composed of ZnSe at the stage at which the phase transition occurs (between 2-6 monolayers), the shell material would be expected to be the primary site of nucleation of this phase transition. This is especially true if the phase transition is related to the solvent system, as the ZnSe shell material would be the only material within the nanocrystal that could interact with the ligands after growth of ~1 ML of shell. However, if strain is the cause of the phase transition, the nucleation site for phase transition could either be in the core material, where the strain is most concentrated, in the shell material, where the strain decays in the outward radial direction, or at the core-shell interface. To examine whether the elastic energy due to strain is able enough to compensate for this phase transition, we have calculated the elastic energy due to strain to be 2.93 eV per QD for a CdTe QD with 0.7 monolayers of spherically concentric shell material. This value increases with shell thickness. Using concentric cylinders, the elastic energy increased to ~4.5 eV. In comparison, the zinc blende to wurtzite transition energy for this heterostructure can be calculated to be ~5 eV, a value that increases much faster than the elastic strain energy with shell thickness. Thus, the elastic energy is insufficient to solely compensate for the energy in this phase transition. There are several potential sources of error in this assessment that could preclude this direct comparison. For example, the phase transition energies have only been theoretically calculated, with little basis for empirical verification, due to the paucity of bulk metastable phases of CdTe and ZnSe. As well, the exact calculation of elastic energy may be impacted by the use of a continuum model for highly faceted nanostructures with relatively few atoms.

Supplementary References:

1. Murray, C. B., Norris, D. J., & Bawendi, M. G. Synthesis and characterization of nearly monodisperse CdE (E = S, Se, Te) semiconductor nanocrystallites. *J. Am. Chem. Soc.* **115,** 8706-8715 (1993).
2. Dabbousi, B. O. et al. (CdSe)ZnS core-shell quantum dots: Synthesis and characterization of a size series of highly luminescent nanocrystallites. *J. Phys. Chem. B* **101,** 9463-9475 (1997).
3. Cao, Y. W. & Banin, U. Growth and properties of semiconductor core/shell nanocrystals with InAs cores. *J. Am. Chem. Soc.* **122,** 9692-9702 (2000).
4. Balet, L. P., Ivanov, S. A., Piryatinski, A., Achermann, M., & Klimov, V. I. Inverted core/shell nanocrystals continuously tunable between type-I and type-II localization regimes. *Nano Lett.* **4,** 1485-1488 (2004).
5. Ivanov, S. A. et al. Type-II core/shell CdS/ZnSe nanocrystals: synthesis, electronic structures, and spectroscopic properties. *J. Am. Chem. Soc.* **128,** 11708-11719 (2007).
6. Adachi, S. *Properties of Group-IV, III-V and II-VI Semiconductors*. (John Wiley & Sons, West Sussex, England, 2005).
7. Toropov, A. A. et al. Coexistence of type-I and type-II band lineups in Cd(Te,Se)/ZnSe quantum-dot structures. *Appl. Phys. Lett.* **89,** 123110-123112 (2006).
8. Chen, C. Y. et al. Spectroscopy and femtosecond dynamics of type-II CdSe/ZnTe core-shell semiconductor synthesized via the CdO precursor. *J. Phys. Chem. B* **108,** 10687-10691 (2004).
9. Yeh, C. Y., Lu, Z. W., Froyen, S., & Zunger, A. Zinc-blende - wurtzite polytypism in semiconductors. *Phys. Rev. B* **46,** 10086-10097 (1992).
10. Wei, S. H. & Zhang, S. B. Structure stability and carrier localization in CdX (X = S, Se, Te) semiconductors. *Phys. Rev. B* **62,** 6944-6947 (2000).
11. Ding, Y., Wang, Z. L., Sun, T. J., & Qiu, J. S. Zinc-blende ZnO and its role in nucleating wurtzite tetrapods and twinned nanowires. *Appl. Phys. Lett.* **90,** (2007).
12. Yu, W. W., Wang, Y. A., & Peng, X. G. Formation and stability of size-, shape-, and structure-controlled CdTe nanocrystals: Ligand effects on monomers and nanocrystals. *Chem. Mater.* **15,** 4300-4308 (2003).
13. Cozzoli, P. D. et al. Shape and phase control of colloidal ZnSe nanocrystals. *Chem. Mater.* **17,** 1296-1306 (2005).
14. Chen, H. et al. Colloidal ZnSe, ZnSe/ZnS, and ZnSe/ZnSeS quantum dots synthesized from ZnO. *J. Phys. Chem. B* **108,** 17119-17123 (2004).
15. Shan, C. X., Liu, Z., Zhang, X. T., Wong, C. C., & Hark, S. K. Wurtzite ZnSe nanowires: growth, photoluminescence, and single-wire Raman properties. *Nanotechnology* **17,** 5561-5564 (2006).
16. Mohamed, M. B., Tonti, D., Al-Salman, A., Chemseddine, A., & Chergui, M. Synthesis of high quality zinc blende CdSe nanocrystals. *J. Phys. Chem. B* **109,** 10533-10537 (2005).
17. Reiss, P. ZnSe based colloidal nanocrystals: Synthesis, shape control, core/shell, alloy and doped systems. *New J. Chem.* **31,** 1843-1852 (2007).
18. Zhong, X. H., Xie, R. G., Zhang, Y., Basche, T., & Knoll, W. High-quality violet- to red-emitting ZnSe/CdSe core/shell nanocrystals. *Chem. Mater.* **17,** 4038-4042 (2005).

19. Adachi, S., Kimura, T., & Suzuki, N. Optical properties of CdTe - experimental and modeling. *J. Appl. Phys.* **74,** 3435-3441 (1993).